

Deep Learning Enhanced Contrast Source Inversion for Microwave Breast Cancer Imaging Modality

Umita Hirose, Peixian Zhu, and Shouhei Kidera , Senior Member, IEEE

Abstract—This study presents a deep-learning (DL) based contrast source inversion (CSI) algorithm for quantitative microwave breast cancer imaging. Inverse scattering analysis for quantitative dielectric profile reconstruction is promising for a higher recognition rate for cancer detection, especially for malignant breast tumors. We focus on CSI as a low complexity approach, and implement a deep convolutional autoencoder (CAE) scheme using radar raw-data, which enhances the convergence speed and reconstruction accuracy. Numerical tests using MRI-derived realistic phantoms demonstrate that the proposed method significantly enhances the reconstruction performance of the CSI.

Index Terms—Convolutional auto-encoder (CAE), contrast source inversion (CSI), deep learning, inverse scattering analysis, microwave ultra wide-band (UWB) breast cancer detection.

I. INTRODUCTION

AS Many reports have indicated as in the world cancer research fund (WCRF) [1], breast cancer is globally recognized as one of the most frequently diagnosed and fatal cancers among women. The most common imaging modality for breast cancer detection is X-ray mammography, however, this method is physically painful due to the high compression of the breast, and is also harmful to cells owing to high energy X-ray exposure, and this is a major factor in a lower screening rate. Several alternative modalities using ultrasound have been developed, such as ultrasonic echo [2] and photo-acoustic imaging [3]; however, these methods have several drawbacks, such as the dependence of recognition rate on the extensive experience of physicians, and the possibility of overlooking malignant tissue due to the difficulty in distinguishing between fibro-glandular tissue and tumors from qualitative ultrasound images.

As an alternative of the above modalities, microwave breast imaging provides a safer and more frequent pre-screening modality characterized by low cost, non-ionizing electromagnetic exposure, non-contact measurement, and compactness. The physical basis of microwave cancer detection relies on the significant contrast between normal adipose and cancerous tissues [4], leading to a distinctive backscattering and a high contrast qualitative image, using confocal qualitative imaging [5].

Manuscript received 14 September 2021; revised 27 October 2021; accepted 7 November 2021. Date of publication 22 November 2021; date of current version 23 August 2022. This work was supported by JSPS KAKENHI under Grant JP20H02161. (Corresponding author: Shouhei Kidera.)

The authors are with the Graduate School of Informatics and Engineering, The University of Electro-Communications, Chofu 182-8585, Japan (e-mail: hirose.umita@ems.cei.uec.ac.jp; zhu.peixian@ems.cei.uec.ac.jp; kidera@uec.ac.jp).

Digital Object Identifier 10.1109/JERM.2021.3127110

However, recent studies have demonstrated that there is a low contrast between fibro-glandular and tumor tissues, at most 10–20% [4], which indicates that existing confocal radar imaging suffers greatly from lower specificity, especially when dealing with highly dense breast tissue.

The tomographic approach is another promising approach that is based on inverse scattering (IS) analysis, in which a complex dielectric profile is numerically reconstructed by solving the domain integral equations. However, this problem is non-linear in nature, and should be solved in mainly ill-posed situations. Thus, there are many IS approaches, such as Born approximation, (equivalent to diffraction tomography), the distorted Born iterative method (DBIM) [6]–[8], (*i.e.*, Gauss-Newton method), or other approaches. As a low complexity approach, a contrast source inversion (CSI) based method was developed [9] and been applied to breast cancer imaging [10], [11], and there are many extensions, such as MR-CSI [12], FD-CSI [13], FEM-CSI, and CSEB [14]. A notable feature of the CSI based method is that it does not require an iterative step using a forward solver, such as FDTD, but optimize both the object function and total electric fields within region of interest (ROI) by introducing the cost function of data and state equation. There have been a number of publications demonstrating its effectiveness for dispersive breast media [11] in terms of lower computational cost and higher accuracy. However, there remains an inherent problem caused by nonlinearity and ill-posedness, especially for the dependency of the initial estimate.

To overcome aforementioned challenges, this study introduces the deep-learning (DL) based initial estimator for a CSI reconstruction scheme. DL is one of the most powerful tools for solving non-linear optimization problems, and there are various DL-based IS solutions in the literature [15]–[21]. A physically inspired prior estimate method has been also developed to solve the inverse scattering problem [22]. However, the accuracy of the above approaches depended significantly on the selected training dataset and did not provide physical constraints, *i.e.*, electromagnetic scattering phenomena, as a later state. Therefore, in this study, a deep neural network (DNN) derived from a deep convolutional autoencoder (CAE) [23] was introduced to convert 1-D scattering data in the frequency domain into 2D complex dielectric profiles to alleviate the problem caused by higher dimension input, *i.e.*, the course of dimensionality, when an insufficient number of training samples was used. Finally, its output is introduced as an initial estimate of CSI, which would significantly enhance a convergence speed and reconstruction accuracy. Although the study in [24] also introduced a CAE

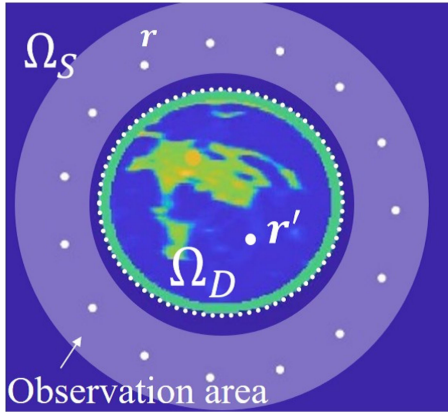


Fig. 1. Observation model. Observation and object areas are defined as Ω_S and Ω_D , respectively.

based reconstruction, it assumed a very simple shaped target with homogeneous media and also a non-dispersive object. These assumptions are unsuitable for biological tissues with highly heterogeneous and dispersive media and cannot guarantee physical relevance. A notable point of our method is the assignment of three Debye parameters to the three-dimensional outputs of each RGB value, which differs from the method in [24]. The 2-D FDTD numerical test, which uses four representative realistic phantoms with different fibro-glandular densities, demonstrates that the proposed approach greatly improves the reconstruction accuracy relative to that obtained by the original CSI method.

II. METHOD

A. Observation Model

Fig. 1 presents the 2-D geometry, including the observation and object area. A number of transmitters and receivers are arranged on the area surrounding breast media, defined as Ω_S . The breast is composed of skin, adipose, fibro-glandular, and cancer tissues, with dispersive and isotropic dielectric properties, the area of which is denoted Ω_D (*i.e.*, the ROI). All combination data between transmitters and receivers are used for the reconstruction scheme. $E_{i,j,k}^T(\mathbf{r})$ and $E_{i,j,k}^I(\mathbf{r})$ denote the total electric field in the case with and without the object, respectively, where the i -th transmitter and j -th receiver are assumed at the k th frequency bin. $E_{i,j,k}^S(\mathbf{r}) \equiv E_{i,j,k}^T(\mathbf{r}) - E_{i,j,k}^I(\mathbf{r})$ is defined as a scattering electric field.

B. Proposed Method

An inverse scattering problem to reconstruct a dielectric profile is a non-linear, and machine-learning-based inversion approaches, such as the DNN [15], have been developed. However, the reconstruction results provided by such methods largely depend on the training dataset and do not necessarily guarantee physical significance in terms of electromagnetic scattering physics. In addition, there are few studies to deal with the dispersive model. To overcome this challenge, here, we combined the DNN-based initial estimator and the CSI post reconstruction scheme. The proposed method consists of three processing steps

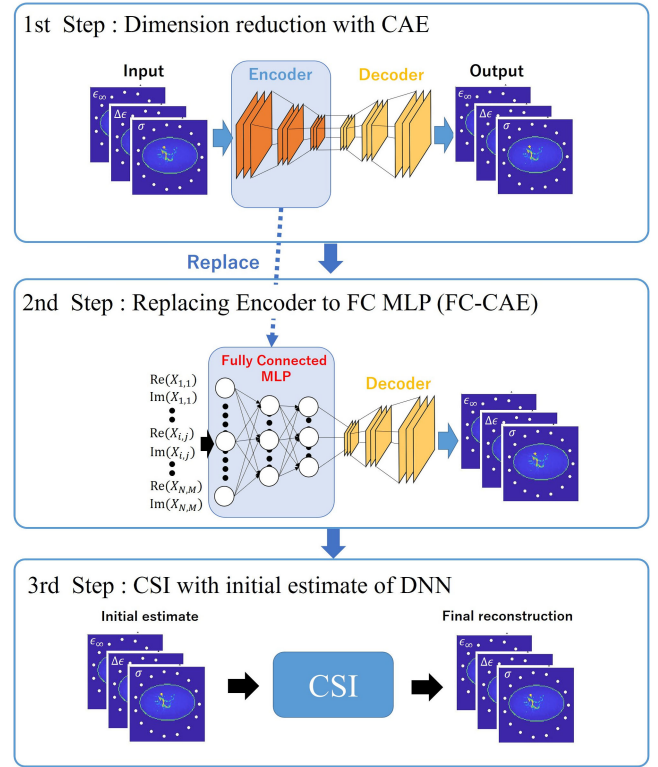


Fig. 2. Schematic processing of the proposed method.

as shown in Fig. 2. First, the 2D Debye parameter profiles were processed in CAE to convert high-dimension data (2D image) into lower-dimension data using the autoencoder feature. In the second step, the trained CAE encoder part was replaced by the fully connected (FC) multilayer perceptron (MLP) network, resulting in a so-called FC-CAE network, to address the 1-D scattered frequency data collected by sensors. In the third step, the trained FC-CAE network provided an initial estimate of the Debye profiles of the input test (scattered) data, which were then processed in the CSI inversion scheme. This third step is a novel point from other DNN-based inversion schemes, that is, the final reconstruction results would satisfy the (electromagnetic) physical conditions.

1) *Initial Estimate by FC-CAE Based Inversion:* Our proposed method first reconstructs the dielectric profile using the FC-CAE-based inversion, and then, the profile is exploited as the initial estimate of sequential CSI processing, namely, updating the result by physical interpretation. Here, the input vector is simply composed of the 1-D complex-valued frequency responses for all combinations of transmitters and receivers, defined as $E_{i,j,k}^S(\mathbf{r})$. To handle dispersive breast media, the following single-pole Debye model was introduced, $\epsilon_{\text{Debye}}(\omega; \epsilon_\infty, \Delta\epsilon, \sigma) = \epsilon_\infty + \frac{\Delta\epsilon}{1+j\omega\tau} + \frac{\sigma}{j\omega\epsilon_0}$, where τ is the relaxation time. The three Debye parameters ϵ_∞ , $\Delta\epsilon$, and σ are then normalized by their corresponding maximum values and converted to red, blue, and green values, respectively, at each pixel of the 2-D image, respectively. At the first step, CAE was processed to reduce the redundant dimensions of the above Debye 2D profile, where the input and output training data

were identical. In the second step, the encoder part of CAE was replaced by the FC-MLP network, which converted the 1D input vectors (scattered data as $E_{i,j,k}^S(\mathbf{r})$) into 2-D Debye profiles, defined as $\chi^{\text{DNN}}(\mathbf{r})$ as shown in Fig. 2. It should be noted that the decoder part of the trained CAE was retained with same weights, while CAE could effectively convert the lower dimensional radar data $E_{i,j,k}^S(\mathbf{r})$ to higher dimensional Debye profiles by reducing the number of redundant dimensions.

2) *Initial Prior-Based CSI Reconstruction*: Finally, as the third step of the proposed method, the FC-CAE based reconstruction result $\chi^{\text{DNN}}(\mathbf{r})$ is input as an initial estimate of the CSI. Here, the CSI solves the two types of domain integral equations expressed as follows:

$$E_{i,j,k}^S(\mathbf{r}) = (k_k^B)^2 \int_{\Omega_D} G_{j,k}^B(\mathbf{r}') w_{i,k}(\mathbf{r}') d\mathbf{r}', (\mathbf{r} \in \Omega_S), \quad (1)$$

$$\begin{aligned} & w_{i,k}(\mathbf{r}) - \chi_k(\mathbf{r}) E_{i,j,k}^{\text{TB}}(\mathbf{r}) \\ &= \chi_k(\mathbf{r}) (k_k^B)^2 \int_{\Omega_D} G_{j,k}^B(\mathbf{r}') w_{i,k}(\mathbf{r}') d\mathbf{r}', (\mathbf{r} \in \Omega_D), \quad (2) \end{aligned}$$

where k_k^B and $G_{j,k}^B(\mathbf{r})$ are the wavenumber and Green's function of the background media, respectively. $w_{i,k}(\mathbf{r}) \equiv E_{i,k}^T(\mathbf{r}) \chi_k(\mathbf{r})$ denotes the dummy variable, called the contrast source, where $\chi_k(\mathbf{r}) \equiv \epsilon_k(\mathbf{r}) / \epsilon_k^B(\mathbf{r}) - 1$ denotes the contrast function. Here, $\epsilon_k(\mathbf{r})$ and $\epsilon_k^B(\mathbf{r})$ denote the complex permittivities of an object and background media, respectively. Equations (1) and (2) are called data and state equations, respectively. Note that, in Eq. (2), the subscript j denotes the position of each cell in the ROI.

To obtain the optimal solution of χ , the CSI minimizes the following cost function at the specific frequency f_k :

$$\begin{aligned} F_k(\chi_k, w_k) &\equiv \frac{\sum_i \|E_{i,j,k}^S - k_k^{B^2} \int_{\Omega_D} G_{j,k}^B w_{i,k} d\mathbf{r}\|_{\Omega_S}^2}{\sum_i \|E_{i,j,k}^S\|_{\Omega_S}^2} \\ &+ \frac{\sum_i \|\chi_k E_{i,k}^{\text{TB}} - w_{i,k} + \chi_k k_k^{B^2} \int_{\Omega_D} G_{j,k}^B w_{i,k} d\mathbf{r}\|_{\Omega_D}^2}{\sum_i \|\chi_k E_{i,k}^{\text{TB}}\|_{\Omega_D}^2}, \quad (3) \end{aligned}$$

where $\|\cdot\|_S^2$ and $\|\cdot\|_D^2$ denote the l_2 norms of the regions Ω_S and Ω_D , respectively. The CSI has a notable feature whereby it simultaneously optimizes not only $\chi(\mathbf{r})$, but also the total field $E_{i,k}^T(\mathbf{r})$ at all cells in the ROI, which can avoid iterative use of a computationally expensive forward solver, such as in the FDTD method. In this method, the DNN based reconstruction $\chi^{\text{DNN}}(\mathbf{r})$ is used to initialize a cost function in Eq. (3), which increases the convergence speed and enhance the reconstruction accuracy.

III. NUMERICAL TEST

A. Numerical Setup

We conducted 2-D FDTD based numerical tests as follows. We introduce four different types (different fibro-glandular density models) of realistic numerical phantoms, as Class 1 (mostly fatty, ID=012804), Class 2 (scattered fibroglandular, ID=070604PA1), Class 3 (heterogeneously dense ID=062204), and Class 4 (very dense ID=012304), which are available from

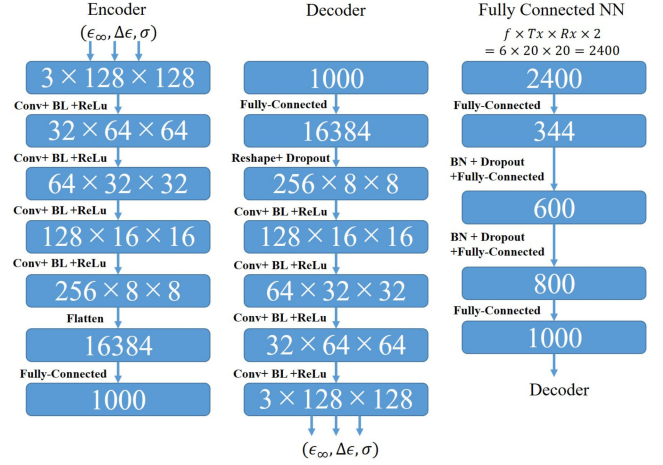


Fig. 3. Structure for CAE and fully-connected NN. If a layer shows the expression as $(Y \times X \times X)$, Y denotes the number of filters and $X \times X$ denotes the size of 2-D data.

open phantom repositories [25] derived from the magnetic resonance imaging (MRI) image associated dielectric profiles. The 20 transmitter and receivers are located in the area surrounding the breast, namely, Ω_S . The source current form is a Gaussian modulated pulse with a 2.45 GHz center frequency with a 2.7 GHz bandwidth. The single pole Debye model is used to express the frequency dependency of complex permittivity, the relevance of which has been demonstrated in the literature [4]. The forward solver is the FDTD method, where the cell size is 2 mm.

B. Results and Discussion

To increase the number of training data, we divide a number of cross-section images from the three-dimensional numerical phantom, with different z , where a 2 mm interval is sampled along the z axis for each phantom. Then, we obtain 172 different 2-D profiles from four classes. Moreover, in order to validate only one inherent systematic error in each reconstruction approach, we assumed that the training and testing data did not include any noise. Fig. 3 shows the detailed network structures of the decoder and encoder of the CAE and FC layers used in the proposed scheme (Fig. 2). In the training phase, a batch learning (BL) and rectified linear unit (ReLU) are introduced to each convolutional layer, as referred in [23], where 10 % validation data are introduced. For an effective dimensional reduction, multiple filters are also introduced in these layers. Here, the adaptive moment estimation (ADAM) [26] algorithm was applied in the training phase. The representative training data are as illustrated in Fig. 4. To increase the dataset and resolve the limited availability of the realistic phantom, we added the data samples by rotating each of the 172 original profiles. The five rotation angles used herein were $0, \pi/4, \pi/2, 3\pi/4,$ and π , and the rotation axis was set at the center of the array. Thus, we were able to extract 860 (172×5) data samples. Three test profiles were constructed (5, 6, and 7), which were extracted from different cross-section profiles of the training data set but with the same ID. In addition, the two test profiles constructed

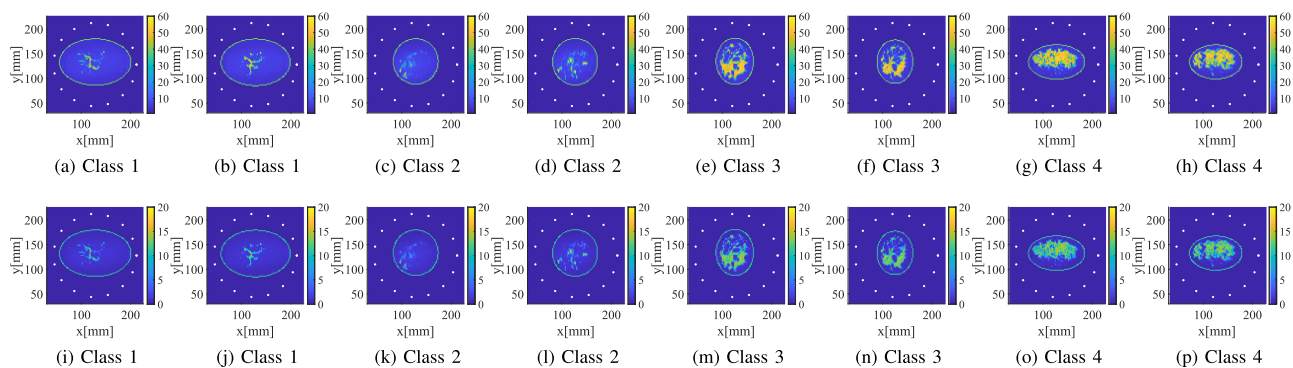


Fig. 4. Training profiles extracted from different classes. White dots denote the transmitters and receivers. Upper and lower lines denote the real and imaginary parts complex permittivity, respectively.

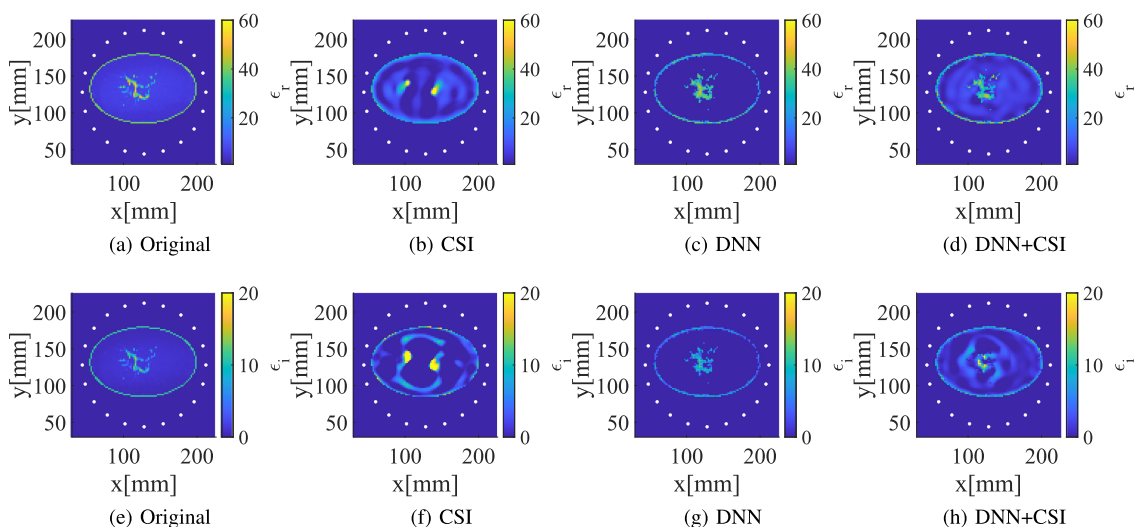


Fig. 5. Reconstruction results of real and imaginary parts of complex permittivity profile in Class 1 (ID=012804). White dots denote the transmitters and receivers. Color denotes each value of complex permittivity.

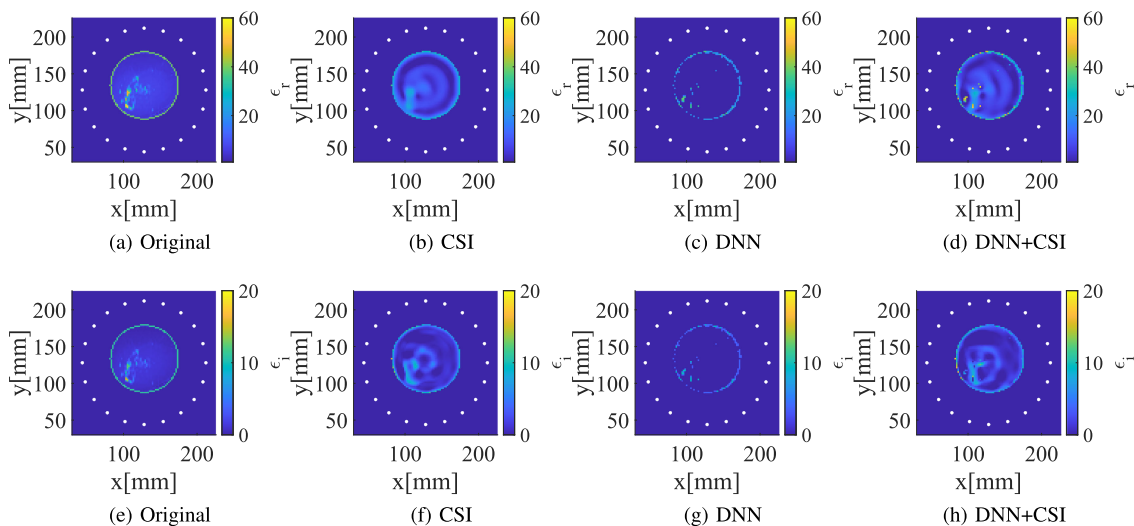


Fig. 6. Reconstruction results of real and imaginary parts of complex permittivity profile in Class 2 (ID=070604PA1).

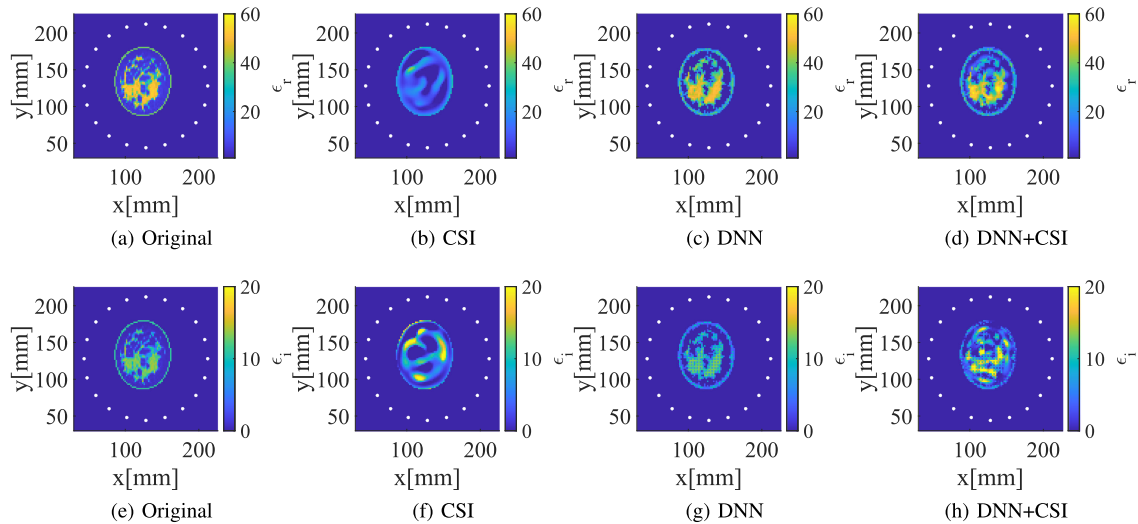


Fig. 7. Reconstruction results of real and imaginary parts of complex permittivity profile in Class 3 (ID=062204).

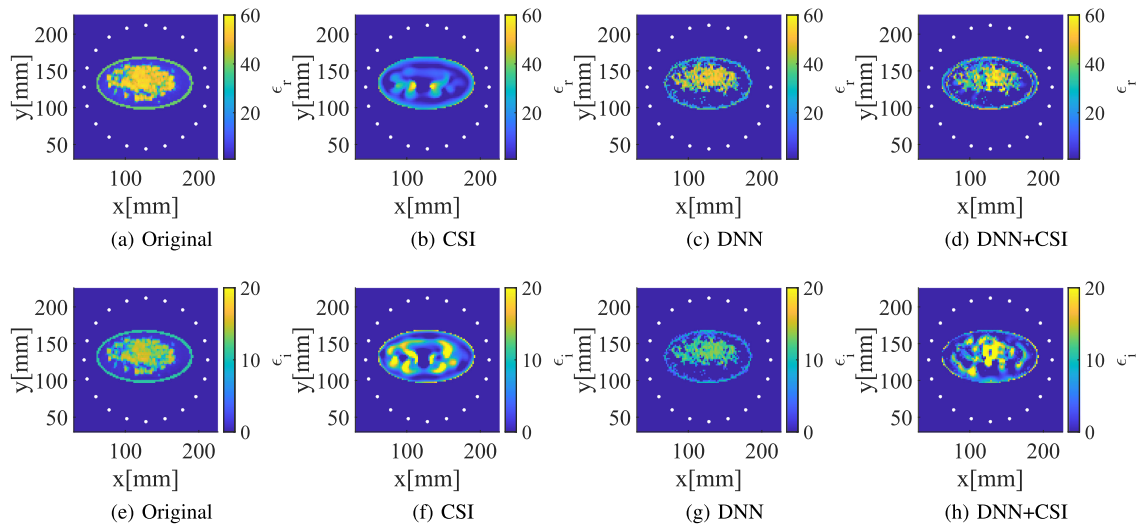


Fig. 8. Reconstruction results of real and imaginary parts of complex permittivity profile in Class 3 (ID=080304).

using different IDs (080304 and 070604PA2) in Class 3 were added to validate the applicability of each method. Thus, a total of five test samples (not included in the training dataset) were examined.

Figs. 5, 6, 7, 8 and 9 present the reconstruction results of the real part of the complex permittivity profiles using five different test cases, by the original CSI, the DNN reconstruction and the proposed method (DNN+CSI), namely, the initial estimate of DNN outputs are introduced into the CSI approach. Note that, the single frequency data at 2.45 GHz is used for the CSI inversion. These results revealed that the DNN-based reconstruction significantly improved the reconstruction accuracy compared to that obtained from the original CSI, without DNN assistance, even in using a limited number of training samples. This is because the CSI reconstruction highly depends on the initial estimate, in such ill-posed condition. In addition, even when phantoms with different IDs from the training data were used as test data,

the proposed method retains the reconstruction, accuracy, which are also relevant with regard to the electro-magnetic scattering physics. The root mean square errors (RMSEs) of these results (except in the skin region) are summarized in Table I. The RMSE is a standard error criterion adopted in many studies, *e.g.*, [27]. This table also showed that the reconstruction accuracy was significantly improved, especially in the real parts of complex permittivity in Classes 1, 3 (ID = 062204 and 080304), and 4. In contrast, the DNN-based reconstruction in Class 2 was relatively worse than that obtained by the original CSI, because the profile of Class 2 was dominated by a low dielectric adipose tissue, which could be accurately provided even in using the original CSI. However, the proposed method compensated for the error in DNN, offering a balanced reconstruction performance between DNN and CSI, thus ensuring physical consistency.

In addition, to quantitatively estimate the similarity between the original and reconstruction profiles, the cross-correlation

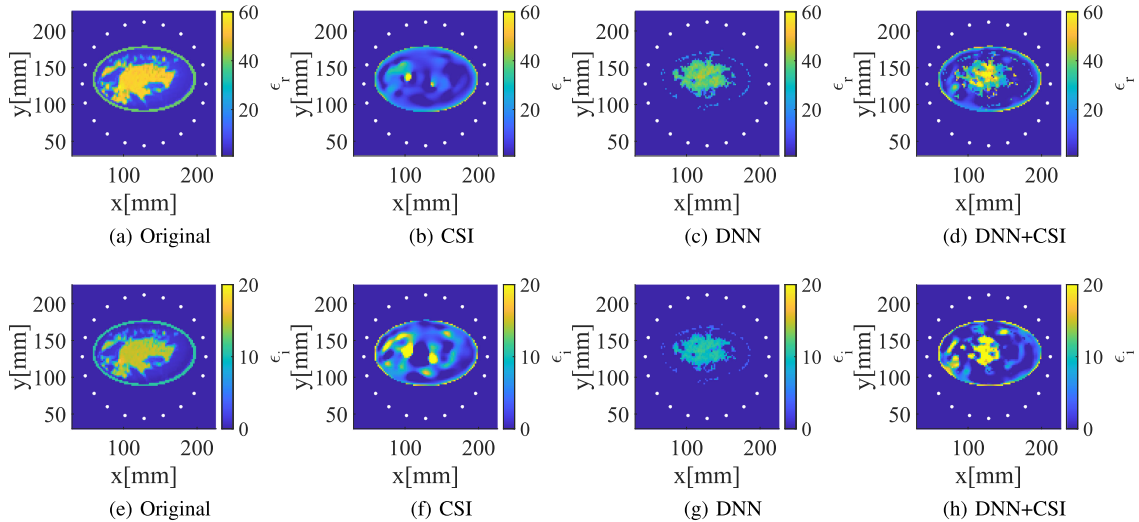


Fig. 9. Reconstruction results of real and imaginary parts of complex permittivity profile in Class 3 (ID=070604PA2).

TABLE I
RMSE FOR RECONSTRUCTION RESULTS OF COMPLEX PERMITTIVITY
AT 2.45 GHZ

		Original	CSI	DNN	DNN+CSI
# 1 (Class 1) ID=012804	Re[ϵ]	10.4	9.4	7.1	
	Im[ϵ]	6.5	3.1	2.6	
# 2 (Class 2) ID=070604PA1	Re[ϵ]	6.9	10.4	7.6	
	Im[ϵ]	2.1	3.1	2.5	
# 3 (Class 3) ID=062204	Re[ϵ]	20.1	17.7	14.2	
	Im[ϵ]	6.8	5.4	6.9	
# 4 (Class 3) ID=080304	Re[ϵ]	24.8	21.2	18.4	
	Im[ϵ]	9.5	6.4	9.2	
# 5 (Class 3) ID=070604PA2	Re[ϵ]	24.7	20.6	19.5	
	Im[ϵ]	9.9	6.5	9.6	

TABLE II
CROSS-CORRELATION COEFFICIENT ρ FOR THE RECONSTRUCTION
RESULTS AT 2.45 GHZ

		Original	CSI	DNN	DNN+CSI
# 1 (Class 1) ID=012804	Re[ϵ]	0.40	0.57	0.70	
	Im[ϵ]	0.23	0.50	0.55	
# 2 (Class 2) ID=070604PA1	Re[ϵ]	0.67	0.52	0.67	
	Im[ϵ]	0.61	0.46	0.60	
# 3 (Class 3) ID=062204	Re[ϵ]	0.40	0.56	0.71	
	Im[ϵ]	0.38	0.45	0.47	
# 4 (Class 3) ID=080304	Re[ϵ]	0.26	0.43	0.54	
	Im[ϵ]	0.25	0.37	0.40	
# 5 (Class 3) ID=070604PA2	Re[ϵ]	0.23	0.37	0.45	
	Im[ϵ]	0.23	0.34	0.37	

coefficient ρ was calculated as follows:

$$\rho = \frac{\chi^{\text{true}} \cdot \chi^{\text{est}}}{\|\chi^{\text{true}}\| \|\chi^{\text{est}}\|}, \quad (4)$$

where χ^{true} and χ^{est} represent the original and reconstruction contrast functions, respectively. This criterion has been widely applied in previous studies [27], [28]. Table II also summarizes the cross-correlation coefficients in each method, and demonstrates that our proposed method would provide more similar dielectric profile pattern especially in highly heterogeneous phantoms. Notably, although the RMSEs of the imaginary-part

reconstructions were inferior to those of the DNN results in Cases # 4 and # 5, the similarity indexes, ρ , increased in both the real and imaginary parts in all the five cases. This demonstrates that the proposed method (DNN + CSI) offers high physical relevance and accurate reconstruction in complex permittivity profiles. Note that, although the number of training samples (860) may be insufficient to provide a reliable initial estimate of the DNN, the CAE based dimensional compression in the DNN scheme could partially address with the above issue, and the post-CSI process could further compensate for its inaccuracy, as particularly demonstrated in Case # 5. It should be noted that the computation time for the training stage by the DNN requires more than 9 hours using Intel(R) Xeon(R) Silver 4110 CPU @ 2.10 GHz, 512 GB RAM, Tesla P40 GPU, while the proposed method requires only 1 s as an additional cost.

IV. CONCLUSION

This study introduces a DL-based inversion approach to provide an accurate initial estimate for the CSI reconstruction scheme. The 1-D raw scattering data are effectively converted to the 2-D Debye profile of breast media via two learning processes: CAE-based feature reduction and replacing fully connected NN layer from the encoding layer of CAE. The proposed method avoids irrelevant reconstruction using only the DL approach by introducing CSI, which guarantees physical reliability. The 2-D FDTD numerical test using realistic numerical phantoms with four different classes, demonstrated that our proposed approach remarkably enhanced the reconstruction accuracy even in highly heterogeneous breast media. Finally, the deep learning approach realizes tomography-based quantitative imaging such as that developed in [27]. However, in the simulation test, the number of training samples was not large enough to examine all possible variants of the actual breast media, as the available realistic numerical phantoms are currently limited. Besides, even in the case of a small number of training samples, the proposed CAE-based dimension reduction scheme could alleviate the problem caused

by the curse of dimensionality to some extent. Thus, the findings of the DNN-based initial estimation approach can provide more physically reliable and accurate reconstruction results. Also, in this study the validation data set has not been introduced in the training phase, indicating that it possibly has an overfitting feature. If we have more data samples, we could check the overfitting analysis, using the validation data, which would possibly provide more accurate results. In addition, a multi-frequency CSI scheme considering a dispersive medium [11], could enhance the reconstruction accuracy and will be therefore explored in a future study to extend the scope of the proposed method.

REFERENCES

- [1] F. Bray, J. Ferlay, I. Soerjomataram, R. Siegel, L. Torre, and A. Jemal, "Global cancer statistics 2018: GLOBOCAN estimates of incidence and mortality worldwide for 36 cancers in 185 countries," *Cancer J. Clinicians*, vol. 68, no. 6, pp. 394–424, Dec. 2018, doi: [10.3322/caac.21492](https://doi.org/10.3322/caac.21492).
- [2] G. A. G. M. Hendriks, C. Chen, H. H. G. Hansen, and C. L. de Korte, "3-D single breath-hold shear strain estimation for improved breast lesion detection and classification in automated volumetric ultrasound scanners," *IEEE Trans. Ultrason., Ferroelect., Freq. Control*, vol. 65, no. 9, pp. 1590–1599, Sep. 2018, doi: [10.1109/TUFFC.2018.2849687](https://doi.org/10.1109/TUFFC.2018.2849687).
- [3] N. Nyayapathi and J. Xia, "Photoacoustic imaging of breast cancer: A mini review of system design and image features," *J. Biomed. Opt.*, vol. 24, no. 12, pp. 1–13, 2019.
- [4] M. Lazebnik *et al.*, "A large-scale study of the ultrawideband microwave dielectric properties of normal, benign and malignant breast tissues obtained from cancer surgeries," *IOP Publishing Phys. Med. Biol.*, vol. 52, pp. 2637–2656, 2007, doi: [10.1088/0031-9155/52/20/002](https://doi.org/10.1088/0031-9155/52/20/002).
- [5] E. J. Bond, X. Li, and S. C. Hagness, "Microwave imaging via space-time beamforming for early detection of breast cancer," *IEEE Trans. Antennas Propag.*, vol. 51, no. 8, pp. 1690–1705, Aug. 2003, doi: [10.1109/TAP.2003.815446](https://doi.org/10.1109/TAP.2003.815446).
- [6] W. C. Chew and Y. M. Wang, "Reconstruction of two-dimensional permittivity distribution using the distorted born iterative method," *IEEE Trans. Med. Imag.*, vol. 9, pp. 218–225, Jun. 1990.
- [7] J. D. Shea, P. Kosmas, S. C. Hagness, and B. D. Van Veen, "Three-dimensional microwave imaging of realistic numerical breast phantoms via a multiple-frequency inverse scattering technique," *Amer. Assoc. Phys. Med.*, vol. 37, no. 8, pp. 4210–4226, Aug. 2010, doi: [10.1118/1.3443569](https://doi.org/10.1118/1.3443569).
- [8] K. Noritake and S. Kidera, "Boundary extraction enhanced distorted born iterative method for microwave mammography," *IEEE Antennas Wireless Propag. Lett.*, vol. 18, no. 4, pp. 776–780, Apr. 2019, doi: [10.1109/LAWP.2019.2902351](https://doi.org/10.1109/LAWP.2019.2902351).
- [9] P. M. van denBerg and A. Abubakar, "Contrast source inversion method: State of art," *Progress In Electromagn. Res.*, vol. 34, pp. 189–218, 2001, doi: [10.2528/PIER01061103](https://doi.org/10.2528/PIER01061103).
- [10] H. Sato and S. Kidera, "ROI limited unknowns reduction based contrast source inversion for microwave breast imaging," *IEEE Antennas Wireless Propag. Lett.*, vol. 19, no. 12, pp. 2285–2289, Dec. 2020, doi: [10.1109/LAWP.2020.3030054](https://doi.org/10.1109/LAWP.2020.3030054).
- [11] H. Sato and S. Kidera, "Noise-robust microwave breast imaging applied to multi-frequency contrast source inversion," *IEEE J. Electromagn., RF, Microw. Med. Biol.*, vol. 5, no. 2, pp. 187–193, Jun. 2021, doi: [10.1109/JERM.2020.3041592](https://doi.org/10.1109/JERM.2020.3041592).
- [12] A. Zakaria and J. LoVetri, "Application of multiplicative regularization to the finite-element contrast source inversion method," *IEEE Trans. Antennas Propag.*, vol. 59, no. 9, pp. 3495–3498, Sep. 2011.
- [13] A. Abubakar, W. Hu, P. M. van den Berg, and T. M. Habashy, "A finite-difference contrast source inversion method," *Inverse Problems*, vol. 24, pp. 1–17, 2008.
- [14] L. Crocco, M. D. Urso, and T. Isernia, "Testing the contrast source extended born inversion method against real data: The TM case," *Inverse Problems*, vol. 21, no. 6, pp. S33–S50, 2005.
- [15] L. Li, L. G. Wang, F. L. Teixeira, C. Liu, A. Nehorai, and T. J. Cui, "DeepNIS: Deep neural network for nonlinear electromagnetic inverse scattering," *IEEE Trans. Antennas Propag.*, vol. 67, no. 3, pp. 1819–1825, Mar. 2019.
- [16] K. H. Jin, M. T. McCann, E. Froustey, and M. Unser, "Deep convolutional neural network for inverse problems in imaging," *IEEE Trans. Image Process.*, vol. 26, no. 9, pp. 4509–4522, Sep. 2017.
- [17] X. Ye, Y. Bai, R. Song, K. Xu, and J. An, "An inhomogeneous background imaging method based on generative adversarial network," *IEEE Trans. Microw. Theory Techn.*, vol. 68, no. 11, pp. 4684–4693, Nov. 2020.
- [18] Y. Zhou, Y. Zhong, Z. Wei, T. Yin, and X. Chen, "An improved deep learning scheme for solving 2D and 3D inverse scattering problems," *IEEE Trans. Antennas Propag.*, vol. 69, no. 5, pp. 2853–2863, May 2021, doi: [10.1109/TAP.2020.3027898](https://doi.org/10.1109/TAP.2020.3027898).
- [19] Z. Wei and X. Chen, "Uncertainty quantification in inverse scattering problems with Bayesian convolutional neural networks," *IEEE Trans. Antennas Propag.*, vol. 69, no. 6, pp. 3409–3418, Jun. 2021, doi: [10.1109/TAP.2020.3030974](https://doi.org/10.1109/TAP.2020.3030974).
- [20] J. E. Fajardo, J. Galván, F. Vericat, C. M. Carlevaro, and R. M. Irastorza, "Phaseless microwave imaging of dielectric cylinders: An artificial neural networks-based approach," *Prog. In Electromagn. Res.*, vol. 166, pp. 95–105, 2019.
- [21] X. Chen, Z. Wei, M. Li, and P. Rocca, "A review of deep learning approaches for inverse scattering problems (invited review)," *Progress In Electromagn. Res.*, vol. 167, pp. 67–81, 2020.
- [22] Z. Wei and X. Chen, "Physics-inspired convolutional neural network for solving full-wave inverse scattering problems," *IEEE Trans. Antennas Propag.*, vol. 67, no. 9, pp. 6138–6148, Sep. 2019.
- [23] B. Hou and R. Yan, "Convolutional autoencoder model for finger-vein verification," *IEEE Trans. Instrum. Meas.*, vol. 69, no. 5, pp. 2067–2074, May 2020.
- [24] W. Shao and Y. Du, "Microwave imaging by deep learning network: Feasibility and training method," *IEEE Trans. Antennas Propag.*, vol. 68, no. 7, pp. 5626–5635, Jul. 2020.
- [25] UWCEM, "Numerical breast phantom repository," [Online]. Available: <https://uwcem.ece.wisc.edu/phantomRepository.html>
- [26] K. Diederik and J. Ba, "Adam: A method for stochastic optimization," 2014, *arXiv:1412.6980*.
- [27] F. Gao, B. D. Van Veen, and S. C. Hagness, "Sensitivity of the distorted born iterative method to the initial guess in microwave breast imaging," *IEEE Trans. Antennas Propag.*, vol. 63, no. 8, pp. 145–154, Aug. 2015.
- [28] M. J. Burfeindt, J. D. Shea, B. D. Van Veen, and S. C. Hagness, "Beamforming-enhanced inverse scattering for microwave breast imaging," *IEEE Trans. Antennas Propag.*, vol. 62, no. 10, pp. 5126–5132, Oct. 2014.

Umida Hirose received the B.E. degree in communication engineering and informatics from the University of Electro-Communications, Tokyo, Japan, in 2019 and the M.E. degree from the Graduate School of Informatics and Engineering, University of Electro-Communications, in 2021.

Peixian Zhu received the B.E. degree in automation engineering from the Shandong University of Technology, Zibo, China, in 2018. He is currently working toward the M.E. degree with the Graduate School of Informatics and Engineering, University of Electro-Communications, Tokyo, Japan. His research interests include electromagnetic tomography and also its applications.

Shouhei Kidera (Senior Member, IEEE) received the B.E. degree in electrical and electronic engineering, and the M.I. and Ph.D. degrees in informatics from Kyoto University, Kyoto, Japan, in 2003, 2005, and 2007, respectively. He has been with the Graduate School of Informatics and Engineering, University of Electro-Communications, Tokyo, Japan, since 2009, and is currently an Associate Professor. His current research interests include advanced radar signal processing or electromagnetic inverse scattering issue for ultra wideband (UWB) three-dimensional sensor or bio-medical applications. In 2016, he was stayed with the Cross-Disciplinary Electromagnetics Laboratory, University of Wisconsin-Madison, Madison, WI, USA, as a Visiting Researcher. From 2017 to 2021, he was a Principal Investigator of the PRESTO Program of Japan Science and Technology Agency (JST). He was the recipient of the 2012 Ando Incentive Prize for the Study of Electronics, 2013 Young Scientist's Prize by the Japanese Minister of Education, Culture, Sports, Science and Technology (MEXT), and 2014 Funai Achievement Award. He is a Senior Member of the Institute of Electronics, Information, and Communication Engineers of Japan (IEICE), Institute of Electrical Engineering of Japan (IEEJ), and Japan Society of Applied Physics (JSAP).